Proceedings of the 5th International Conference on Materials Chemistry and Environmental Engineering
DOI: 10.54254/2755-2721/2025.28751

Design and Optimization Model of a Photovoltaic Cogeneration System for Remote Areas: A Case of China

Yonghan Jiao[1*†], Yunting Du[2†], Zhifan Ye[3†], Mingxuan Wang[4#], Jiayu Liu[5#]

[1]*School of Energy and Power Engineering, Xi'an Jiaotong University, Xi'an, China*
[2]*Faculty of Arts and Humanities, University College London, London, United Kingdom*
[3]*Department of Mechanical Engineering, University of Nottingham, Ningbo, China*
[4]*High School Affiliated to Nanjing Normal University Jiangning Campus, Nanjing, China*
[5]*Wuhan Britain-China School, Wuhan, China*
**Corresponding Author. Email: 2216113420@stu.xjtu.edu.cn*
[†]*These authorscontributed equally to this work and should be considered as co-first author.*
[#]*These authorscontributed equally to this work and should be considered as co-second authors.*

Abstract. This study presents the design and optimization of a photovoltaic-thermal cogeneration system aimed at improving energy efficiency and addressing power supply challenges in remote areas of China. The system integrates photovoltaic (PV) panels with phase-change materials (PCM) for waste heat recovery, battery energy storage, and heat pumps, providing both electricity and heat. An optimization model based on regional climate conditions and energy demands was developed, utilizing the interior point method to minimize system costs. The model was tested in three provinces with diverse energy needs: Tibet, Shaanxi, and Hainan. Results show that the system significantly improves the efficiency of PV panels by mitigating heat buildup and reduces total system costs by approximately 30% compared to traditional PV systems. The study highlights the dual-functionality of the system, supplying both electricity and heat while addressing the intermittency of solar power generation through combined battery and thermal storage. The proposed system provides a scalable, cost-effective energy solution for remote areas, offering potential applications in regions with similar climatic and infrastructural challenges.

Keywords: Photovoltaic-Thermal (PV-T) system, Optimization Model, Remote Areas Electrification, Distributed energy system, Phase Change Materials (PCM), Heat Recovery, Battery Energy Storage.

Nomenclature

$\dot{Q}$	Heat transfer rate(W)	$NOCT$	Nominal Operating Cell Temperature (℃)
T	Temperature(℃)	PV	Photovoltaic panel
R_{th}	Thermal resistance (K/W)	HR	Heat Recovery

© 2025 The Authors. This is an open access article distributed under the terms of the Creative Commons Attribution License 4.0 (https://creativecommons.org/licenses/by/4.0/).

DOI: 10.54254/2755-2721/2025.28751

Table. (continued)

k	Conduction coefficient (W/mK)	HS	Heat Storage
h	Convection coefficient ($W/(m^2 \cdot K)$)	BS	Battery Energy Storage
S	Insolation level by solar panels(mW/cm^2)	HP	Heat Pump
E	Efficiency (%)	AA	Ambient Air
v	Wind speed (m/s)	HPHS	Heat Pump of Heat Storage
Δx	Distance of heat transfer (m)	HPAA	Heat Pump of Ambient Air
A	Area (m^2)	HSP	Heat Storage Peak
Ra_L	Rayleigh number	HSV	Heat Storage Valley
Nu	Nusselt number	BSP	Battery Energy Storage Peak
Pr	Prandtl number	BSV	Battery Energy Storage Valley
H	Specific length (m)	OPV	Output from PV
L	Length of the space (m)	PVC	From PV to Consumption
g	Acceleration of the earth (m/s^2)	HIS	Heat Input to Storage
C_p	Heat capacity ($KJ/(kgK)$)	HOS	Heat Output from Storage
d	Specific length (m)	CAPEX	Unit Capital Expenditure
w	Energy (J)	COP	Coefficient of Performance
m	Mass (kg)		Greek symbols
t	Time (s)	Δ	Difference
Cap	Capacity of facility (kW or kWh)	γ	Temperature Coefficient
Le	Storage level (kWh)	v	Kinematic viscosity (m^2/s)
C	Cost (US $)	α	thermal diffusivity (m^2/s)
P	Power (kW)	β	Coefficient of thermal expansion (K^{-1})
	Subscript & Abbreviations		
PCM	Phase changed material		

1. Introduction

Over the past few decades, China has made significant achievements in building power infrastructure and advancing electrification. As the country's socioeconomic development accelerates, the demand for electricity in remote areas has also increased significantly. However, the existing grid can no longer meet the needs of these regions. In rural areas, the issue of power supply continues to seriously affect the quality of life and economic development of local residents.

The problems in remote areas primarily manifest in the following aspects: high line losses and low power quality. Due to technological limitations and overloaded lines [1], there is a significant waste of energy, and voltage quality cannot be guaranteed. In China's remote rural areas, the grid loss rate is typically between 10% and 15%, whereas in developed countries like the U.S. and Japan, it is less than 5% [2]. Some mountainous areas suffer from poor power voltage quality, where user-end voltage often falls below 220V and can drop to 160V to 180V during peak loads [3], causing

DOI: 10.54254/2755-2721/2025.28751

household appliances to malfunction. Additionally, there are serious issues of non-standard electricity use, such as improper placement of distribution boxes and meters, and illegal wiring, which not only reduce equipment lifespan but also pose safety hazards. Furthermore, residential wiring is often substandard due to the lack of professional guidance, increasing grid safety risks. Aging grid infrastructure in some regions, coupled with outdated equipment, further compromises the reliability of power supply. Despite China's significant advancements in long-distance transmission technologies, the costs remain high, making it challenging to upgrade the grid to cover these remote areas comprehensively [4]. In this context, establishing distributed energy and microgrids in remote regions has become a potential solution [5]. China's northwest (e.g., Tibet, Gansu) and southern regions (e.g., Hainan) have abundant solar resources, making it feasible to build photovoltaic (PV) systems tailored to the specific energy needs of these areas [6].

However, despite the advantages of solar PV in regions with ample sunlight, there are technical challenges that impact the performance of these systems and the quality of power supply in distributed energy setups. In practice, only 15% to 22% of solar energy can be converted to electricity by PV panels, with most of the remaining energy manifesting as heat, which raises the temperature of the panels [7]. This heat buildup effect not only reduces PV efficiency but also accelerates the aging of the equipment, shortening its lifespan. Typically, every 1°C increase in panel temperature results in a 0.4% to 0.5% drop in efficiency. Current technologies to address this issue include natural cooling, forced cooling, phase-change materials, and photovoltaic-thermal (PV-T) systems. These methods aim to reduce heat accumulation and explore ways to effectively use the residual heat to enhance the overall efficiency of the PV system [8,9]. The PV-T system, in particular, enables simultaneous power generation and heat utilization for applications like building heating and agricultural greenhouses.

The intermittent and fluctuating nature of PV power generation poses additional challenges. Solar power generation halts during nighttime and cloudy days due to natural weather conditions [10], and its output can vary significantly due to short-term factors like cloud movement. These fluctuations increase the grid's operational burden and can lead to power shortages or energy waste when generation exceeds storage capacity [11]. To address these challenges, energy storage systems, smart grids, and hybrid energy solutions are increasingly being adopted to balance supply and demand and enhance energy efficiency. For localized microgrid systems, deploying battery storage on the generation side is the most effective way to mitigate PV intermittency and mismatch between generation and consumption.

This study identifies the following research gaps based on the current issues in remote areas and solar PV technology:

1. Inadequate grid coverage in remote areas, where outdated infrastructure leads to poor power quality and unstable voltage, especially during peak hours. High transmission costs hinder comprehensive grid upgrades in these regions, affecting both the stability of power supply and economic development.

2. Low efficiency and aging issues in PV systems: Even in areas with high solar irradiance, PV efficiency remains low, typically converting only 15% to 22% of sunlight to electricity. The heat buildup effect reduces efficiency and accelerates aging, compromising long-term reliability.

3. Intermittency and fluctuations in PV generation make continuous power supply challenging, especially during night or overcast conditions. These variations complicate grid management and can lead to wasted energy when excess generation cannot be stored.

The study systematically designs a solar photovoltaic-thermal cogeneration system to address these challenges in various remote areas in China, contributing the following:

DOI: 10.54254/2755-2721/2025.28751

1. A photovoltaic-thermal system design that integrates phase-change materials for heat transfer and storage, combined with heat pumps, battery energy storage, and thermal storage to address heat buildup and meet thermal demands.

2. An optimization model for system configuration based on the climatic and energy requirements of different regions, aiming to minimize system costs using an interior point method.

3. A configuration strategy for battery and thermal storage to maximize solar energy utilization by addressing its intermittency and fluctuations.

This paper will follow the following logic: The second section of this paper will provide a detailed description of the system the research designed, including its working principles and the physical phenomena involved. The third section will focus on simplifying and analyzing the optimization model of our system from both mathematical and physical perspectives, including necessary assumptions, data preprocessing, and a detailed description of the optimization problem and its solution. The fourth section will present the data and results obtained from our optimization model, comparing the performance with that of traditional systems. The fifth section will summarize the research findings and discuss potential areas for improvement in future research.

2. System design and description

The operating principle diagram of the system our research designed is shown in Fig.1.

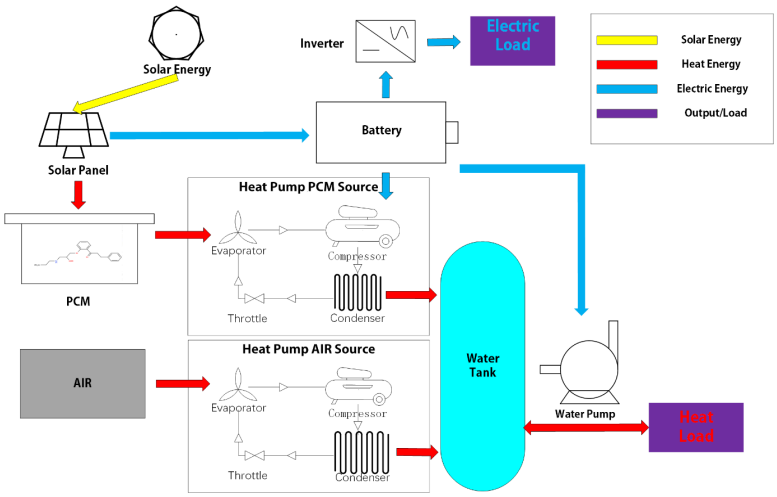

Figure 1. System model

The solar photovoltaic panels in the system are responsible for converting solar energy into electricity. After sunlight hits the photovoltaic panel, the photovoltaic cell converts part of the solar radiation into electricity. Its energy conversion can be expressed by the following formula (1):

$$P = A \times G \times E_0 \times (1 + \gamma \times (T_{cell} - T_{ref})) \tag{1}$$

Where P is the power generation of photovoltaic panels, A is the area of the PV panels. E_0 is the default power generation efficiency of photovoltaic panels, which is affected by the temperature of the photovoltaic panel T_{cell}. γ is temperature coefficient.

Due to the low conversion efficiency of actual photovoltaic panels, usually only 15%-22% of the solar energy is converted into electricity [7], and the rest of the energy is left on the photovoltaic panel in the form of heat, which causes the temperature of the photovoltaic panel to rise. To improve

DOI: 10.54254/2755-2721/2025.28751

power generation efficiency and prevent equipment from overheating, the system incorporates waste heat recovery technology to deal with this heat.

The electricity generated by the photovoltaic part is stored in the battery to cope with the instability and intermittency of solar power generation. Due to the volatility of solar energy, such as at night or in rainy weather, photovoltaic panels cannot produce electricity, so battery energy storage systems are key to ensuring the continuity of power supply. The battery system is used to store electrical energy when solar power is sufficient and to provide electricity when photovoltaic power is insufficient to ensure the stability and continuity of the power load demand.

The majority of the solar energy absorbed by solar panels is converted to heat, and some of that heat is diffused to the surroundings. The other part of the heat is transferred from the backplane to the PCM. n-Hexadecane(C16) of paraffinic, was chosen based on the using situation [12]. It has the advantage of being stable and inexpensive. Ideally, from the start of the daytime, the temperature of the solid and low temperature paraffins are gradually increased by the heating of the solar panels. When the temperature of the paraffin wax reaches the melting point, the paraffin wax will change from a solid state to a liquid state. This phase change process will absorb a lot of energy, which is called Latent heat. The heat generated by solar panels is stored in paraffin and will be used by the heat pump. The heat pump is a reverse structure of air conditioner. The flow in the pipe is refrigerant R-134a which has low phase change temperature. Refrigerant pressure is reduced by the compressor and absorbs the heat of PCM in the evaporator part. This low pressure and relatively high temperature in evaporator environment cause the refrigerant to evaporate and store significant heat energy. The pressure will increase and release heat to the cold water in the condenser part. The high pressure and relatively low temperature result refrigerant easy to condense and the latent heat which is stored in evaporator will be transferred to water. The high-pressure and low-pressure environments in the pipeline are separated by throttle. Finally, heated water is pumped by the water pump and transported to residents and facilities to use.

Heat transfer can be divided into power, which is temperature difference and thermal resistance which is determined by the Properties and geometry of the thermally conductive substance. The heat transfer equation can be expressed by the following equation (2):

$$\dot{Q} = \frac{\Delta T}{R_{th}} \tag{2}$$

Where ΔT is temperature difference and R_{th} is thermal resistance.

The thermal resistance can be described by equation (3) and (4):

$$R_{th} = \frac{\Delta x}{kA} \ (\text{conduction}) \tag{3}$$

$$R_{th} = \frac{1}{hA} \, (\text{convection}) \tag{4}$$

Where Δx is the distance the heat transfer through the solid, k is the conduction coefficient, and h is convection coefficient.

The system effectively solves the intermittency and heat accumulation problems of photovoltaic power generation, and realizes the maximum utilization of solar energy. It not only improves the energy conversion efficiency, but also meets the heat demand through waste heat recovery, improving the energy utilization efficiency of the overall system. By combining photovoltaic power

DOI: 10.54254/2755-2721/2025.28751

generation, battery energy storage, waste heat recovery and heating systems, this system can provide reliable power and heating services to remote areas with high feasibility and economy.

3. Data preprocessing and optimization model ideas

3.1. Case selection and data preprocessing

This study selected three different provinces in China (Tibet, Hainan, and Shaanxi) aiming for higher reliability of the model as well as the higher generalizability of the study. Three provinces are selected based on differences between their electricity and heat demands. For instance, the electricity demand is lower than the heat demand in Tibet whereas the electricity demand is considerably higher than the heat demand in Hainan. For Shaanxi, the electricity demand is relatively equal to the heat demand [13-15]. Differences between the electricity demand and heat demand in three provinces are subject to climate, economic, and social factors [16,17].

Annual solar exposure data and heat demand estimates for these three provinces are easily and reliably available through literature or through the Renewable Ninja website. `However, in terms of data preprocessing, it is difficult to obtain accurate electricity consumption data for the three provinces. Based on the data our research found and considering the characteristics of residential electricity usage, our research used the following method to estimate the hourly electricity consumption data for each of the three provinces over the course of a year. firstly, the data for residential annual maximum electricity load curves and residential annual maximum electricity load curves are acquired from the government report which contain each province in China [18]. However, the line charts revealed in the report is not sufficient to locate value of electricity load for each hour on the curves. Therefore, piecewise fitting is used to find precise values of electricity load for each hour on annual maximum electricity curves for the three provinces.

The annual maximum load curve for each province is fitted via MATLAB. Firstly, considering the accuracy of the fitted curves, the data collected is split into small data sets. There are four fit types involved, including polynomial, exponential, logarithmic and Fourier. The best fit type is chosen based on the R-square value when it is higher than 0.9. In this case, by taking 57 sets of feature points from the annual maximum load curves and input the data sets as column vector into MATLAB, 9 sections of the annual maximum load curves for each province are generated and combined together for further result analysis. Our research finally obtained the piecewise function fitting results as shown in the appendix. The fitted electricity curves' functions are included in Appendix1-Fitted Curves. The fitted electricity load curves for the three provinces are presented in Fig. 2 below:

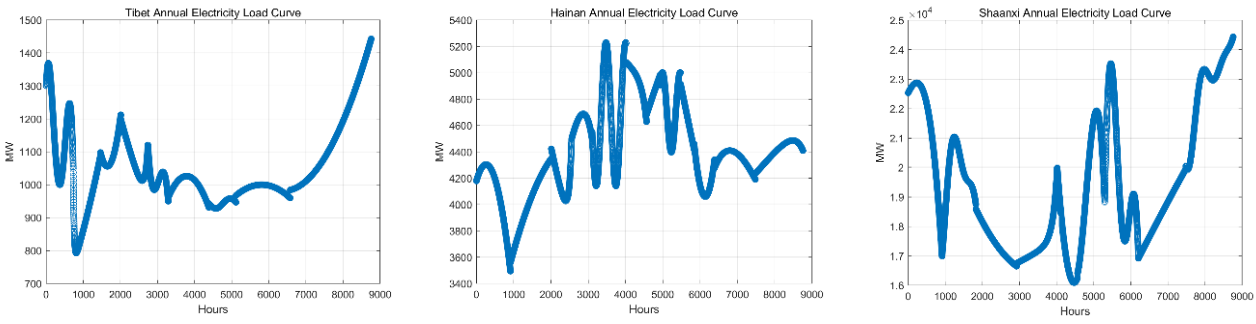

(a) Tibet's (b) Hainan's (c) Shaanxi's

Figure 2. Fitted electricity load curves of the three provinces

DOI: 10.54254/2755-2721/2025.28751

However, for the broadly application of the model, further supplementary data processing should be established for a more realistic annual residential electricity load curve. Therefore, the typical 24 hours residential daily electricity load curve is used to form the typical annual residential electricity load curve. The process involves splitting the 8760 data sets into 365 groups of data sets and there are 24 data sets for each group. Then, by taking into account the maximum value from the typical 24 hours residential daily electricity load curve and its corresponding time, the proportion is calculated against the value corresponds the same time from the fitted residential annual maximum electricity load curves. The remaining 23 values are changed in proportion, with the same 'proportional scaling' method applied into all 365 groups to result in electricity load curves, which illustrates the residential electricity load for each hour.

In addition to the simulation, the study also takes into consideration of applying a typical 24 hours four-people electricity load curve of each four to generate the four different electricity curves for each hour. For each province, a typical four seasons four-people family electricity curve is going to take the maximum value and with same methods in generating the typical 24 hours residential daily electricity load curves. In this case, it is revealed that the 'proportional scaling' explained previously is also applied for precisely producing a typical seasonal electricity load curve. Based on analysis above, our research obtain the annual electricity load curves of the three provinces, and the hourly load curves of one month (July) of the three provinces are captured and displayed in Fig. 3 below:

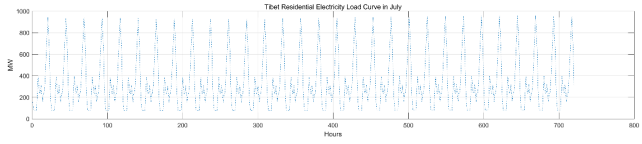

(a) Tibet's

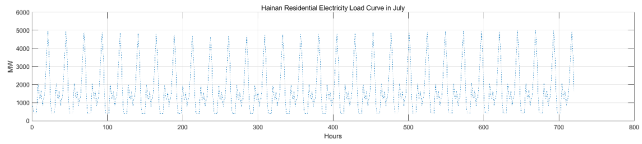

(b) Hainan's

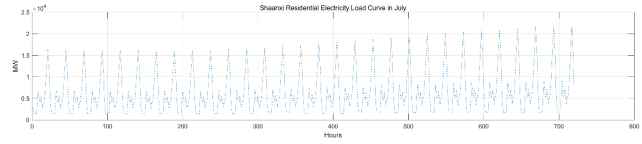

(c) Shaanxi's

Figure 3. Load curves of one month (July) of the three provinces

The final residential electricity load curves of three provinces are obtained by dividing the total numbers of residents in each province and multiple 2000, which is the sample size of the study. The final residential electricity load curves and the typical 24 hours residential daily electricity load curves of three provinces in four seasons are included in Appendix1-Load Data.

DOI: 10.54254/2755-2721/2025.28751

3.2. Assumptions and parameters estimation

To build an optimization model for the system our research described, we need to abstract the physical processes into mathematical representations. Since the physical processes involved in the system are highly complex and the inputs and desired outputs of our optimization model are general data, it is necessary to pre-calculate many of the parameters outside of the optimization model and input them into the model. Additionally, certain simplifications and assumptions must be made about the system to ensure that the designed model is applicable and universally valid. In this experiment, the day was divided into two parts. One of that is daytime which was set from 9:00 to 17:00 which is a total of 8 hours, and the rest of the day was nighttime. Filtering the average temperatures through the temperature recordings [19], the average daytime temperature and night temperature can be gotten. The experiments were also simplified by the recorded light data [19]. Solar energy only be applied in the daily time, which is between 6:00 to 17:00 so the daytime radiation can be gotten, and in night they are all 0 W/ m^2 . The corresponding average wind speed can be obtained [19]. The detailed data has been put into the Appendix2.

The solar panel named PV SOL60P-260W with product code MA- 0532 was used,and the data of it is operated as the assumption [20].

The temperature of a standard solar panel can be obtained from the following equation [21]. Where the NOCT is Nominal Operating Cell Temperature and S is S = insolation level by solar panels in mW/cm^2 . The calculation equation (5) is presented below:

$$T_{cell} = T_{air} + \frac{NOCT-20}{80} S \tag{5}$$

The dimension of the solar panel is 1640 x 992 x 45mm. So, the surface area of it is 1.62688 m^2 .

Conventional solar panel cell temperatures can be calculated by equation (5). The result of cell temperature without PCM is shown in Appendix2.

The Module efficiency of the solar panel was tested at a cell temperature of 25 ℃ . The temperature coefficient of the solar panel can be used to calculate the current efficiency [22]. The standard module efficiency of the solar panel is 16% and the temperature coefficient is -0.45%. $E_{electricity}$ is electric efficiency. The efficiency can be calculated by the equation (6) below:

$$E_{electricity} = 0.16 \times [1 - 0.0045 \times (T_{cell} - 25)] \tag{6}$$

So, the electric efficiency without PCM of these three locations can be gotten which is in Appendix2.

However, in this experiment, the cell's heat will be transport through back side of panel into the PCM to be stored. This means that the temperature of the cell will be lower, and the equation (5) which calculates the cell temperature would not be appropriate in this situation.

In order to obtain the heat transfer of each component in the new scheme, it is necessary to calculate the thermal resistance of each part.

To calculate the thermal resistance of air to solar panels requires data of the convection coefficient of air, which can be calculated using the following equation (7) [23]. Where v is the wind speed and h_c is the air convection coefficient.

$$h_c = 10.45 - v + 10 \times v^{\frac{1}{2}} \tag{7}$$

DOI: 10.54254/2755-2721/2025.28751

Therefore, the air convection coefficient of these three provinces can be calculated and put into Appendix2.

In order to calculate the thermal resistance of solar panels, the construction of solar panels needs to be simplified. 95% of solar panels consist by silicon [24] so it is reasonable to consider the panel as objects composed entirely of silicon, when the thermal resistance be calculated.

The thermal conductivity k of silicon at 35℃ is about 145 $W/(m \cdot K)$[25]

Assuming that the solar panel heats up at the centre point. The thermal resistance of heat released from panel to air can be determined by equation (8) below:

$$R_{top} = \frac{\Delta x}{k_{Si} A_{top}} + \frac{1}{h_c A} \tag{8}$$

The thermal resistance on the top and sides of the solar panel can be calculated. Where side1 has the longer length and side2 has shouter one. All these thermal resistance data has been put into the Appendix2.

Convection coefficient of PCM should be gotten to calculate the thermal resistance between solar panel to PCM. Yassine Cherif et al. analysed the Nusselt number of liquid paraffinic in Rectangular closed container with consideration of natural convection, which is similar to the situation in this experiment [26].

The Nusselt number can be obtained by the following equation (9):

$$Nu = 0.42 Ra_L^{\frac{1}{4}} + Pr^{0.012} \left(\frac{H}{L}\right)^{-0.3} \tag{9}$$

Where Ra_L is Rayleigh number, Pr is the Prandtl number, H is the specific length, L is the length of the space.

The value of Rayleigh number can be derived from the following equation (10):

$$Ra_L = \frac{g\beta \Delta T_{PCM-panel} L^3}{v\alpha} \tag{10}$$

Where g is acceleration of the earth which is $9.81 m/s^2$, β is the coefficient of thermal expansion of liquid n-Hexadecane which is $7.664 \times 10^{-4} K^{-1}$. Kinematic viscosity v is about $4.2746 \times 10^{-6} m^2/s$ [27]. To obtain the value of Ra_L , we need to calculate the value of α from the equation (11) below:

$$\alpha = \frac{k}{\rho C_p} \tag{11}$$

C_p is heat capacity which is $485.8 J/(molK)$ and the molar mass is 226g/mol, so the heat capacity is $2.148 KJ/(kgK)$[28].

k is Thermal conductivity which is$0.14 W/mK$[29]. Density$\rho = 770 kg/m^3$

α is the thermal diffusivity and its value is $8.4645 \times 10^{-8} m^2/s$ [28]. Pr is the Prandtl number can be gotten by the following function (12):

$$Pr = \frac{v}{\alpha} \tag{12}$$

So, we can calculate that $Pr = 50.5$.

DOI: 10.54254/2755-2721/2025.28751

To simplify Nu and Ra_L , the height of the PCM needs to be fixed. Assuming that a solar panel corresponds to a paraffin storage container with a height of $50mm$. Rayleigh number can be calculated by equation (13):

$$Ra_L = 2.6 \times 10^6 \Delta T_{PCM-panel} \tag{13}$$

The Nusselt number can be obtained by the equation (14):

$$Nu = 16.86 \Delta T_{PCM-panel}{}^{\frac{1}{4}} + 0.4 \tag{14}$$

The convective conductivity coefficient h can be gotten by the following equation (15):

$$Nu_d = \frac{hd}{k} \tag{15}$$

Where d is specific length which is the same as H and can be calculated by following equation (16):

$$d = \frac{4A}{2(1.64+0.992)} = 1.236m \tag{16.1}$$

$$h = 1.91 \Delta T_{PCM-panel}{}^{\frac{1}{4}} + 0.045 \tag{16.2}$$

Assuming that the night paraffin temperature eventually reaches the night air temperature, which means this structure always has higher COP than the pure air source heat pump.

It is reasonable to calculate how many kilograms of PCM for one heat pump to store the heat deeded in the night.

Vitocal 300-A specification AWO 302.B60 heat pump [12] has been chosen to be a paradigm of the heat pump used in the whole system, calculated based on output as maximum heat, which is 55.8kW.

The amount of heat stored per kilogram of paraffin can be calculated using the latent heat of PCM and the temperature of it should be right lower than the melting point to ensure the heat transfer efficiency. The latent heat of PCM is 237kJ/kg.

The volume of the PCM thermal storage cell corresponding to one solar panel is $0.081344m^3$. The density of PCM is $770kg/m^3$. The mass of PCM for one solar panel is $62kg$.

In order to calculate the energy transfer during the daytime when the heat transfer is in steady state, it is necessary to fix the number of solar panels corresponding to a single heat pump. Assuming that the total number of solar panels is $n = 1000$.

The heat balance of the PCM can now be used to calculate the temperature difference between the PCM and the panel. Vacuum insulation panels have been used to isolate PCM. It has very low Thermal conductivity, so it can assume that no heat transfer through it.

Calculate the thermal resistance from the solar panel to the PCM:

$$R_{panel-PCM} = \frac{\Delta x}{k_{Si} A_{top}} + \frac{1}{hA} \tag{17.1}$$

DOI: 10.54254/2755-2721/2025.28751

$$R_{panel-PCM} = 9.538 \times 10^{-5} + \frac{1}{1.62688 \times \left(1.91 \Delta T_{PCM-panel}{}^{\frac{1}{4}} + 0.045\right)} \tag{17.2}$$

The absorbed energy by heat pump for each PCM structure is $\frac{55800}{1000} = 55.8W$.

Calculate the temperature difference from the plate to the PCM using the energy balance in a steady state.

$$\frac{\Delta T_{PCM-panel}}{R_{panel-PCM}} = 55.8 \tag{18.1}$$

$$\Delta T_{PCM-panel} = 9.98 \tag{18.2}$$

Polycrystalline solar panels have a reflectivity of 0.25%-0.4% [30]. so, it is reasonable to assume the reflectivity is 0.3%. The heat generation efficiency can be found.

$$E_{heat} = 100\% - 0.3\% - E_{electricity} \tag{19.1}$$

$$E_{heat} = 0.819 + 7.2 \times 10^{-4} T_{cell} \tag{19.2}$$

The actual solar energy received by panels can be calculated from the following equation. Where S is average insolation in area.

$$S_{cell} = A \times S \tag{20}$$

The insolation in each solar panel can be determined which is in Appendix2.

Get the heat source from cell:

$$\dot{Q}_{cell} = S_{cell} \times E_{heat} \tag{21.1}$$

$$\dot{Q}_{cell\ Tibet} = 1031.29 + 0.91 T_{cell} \tag{21.2}$$

$$\dot{Q}_{cell\ Xi'an} = 687.53 + 0.60 T_{cell} \tag{21.3}$$

$$\dot{Q}_{cell\ Hainan} = 623.57 + 0.55 T_{cell} \tag{21.4}$$

$$\dot{Q}_{air} = \frac{\Delta T_{panel-air}}{R} \tag{21.5}$$

Using the energy balance equation:

$$\dot{Q}_{cell} = \dot{Q}_{air\ top} + \dot{Q}_{air\ side1} + \dot{Q}_{air\ side2} + 55.8 \tag{22}$$

So, the cell temperature with PCM can be calculated. The result is in Appendix2.

DOI: 10.54254/2755-2721/2025.28751

The heat efficiency and electric efficiency can be gotten by equation (6) in precedent content and equation (23) below. The calculated results are showed in Table 1 and Table 2 :

$$E_{HR} = \frac{55.8}{S_{cell} \times E_{heat}} \tag{23}$$

Table 1. Efficiency of PV panels in three provinces

Parameter	Value
Efficiency of PV panels in Tibet (%)	15.65
Efficiency of PV panels in Shaanxi (%)	15.47
Efficiency of PV panels in Hainan (%)	14.88

Table 2. Efficiency of heat recovery panels in three provinces

Parameter	Value
Efficiency of heat recovery in Tibet (%)	5.27
Efficiency of heat recovery in Shaanxi (%)	7.89
Efficiency of heat recovery in Hainan (%)	8.64

Vitocal 300-A specification AWO 302.B60 heat pump has COP 4.0 at 7℃ air temperature and 3.6 at 2℃ air temperature, and output 35℃ water [29].

Assuming the relationship between the COP of a heat pump and the temperature of the heat source as a function, which can be shown in the equation (24) below:

$$COP_{current} = 0.08T + 3.44 \tag{24}$$

The average COP can be calculated based on the percentage of operating time at the corresponding COP, which can be expressed:

$$COP = \sum \left(COP_n * \frac{t_n}{t_{total}} \right) \tag{25}$$

The temperature of PCM in a steady state in daytime can be obtained:

$$T_{PCM} = T_{cell} - \Delta T_{PCM-panel} \tag{26}$$

The temperature of PCM in three locations can be gotten in Appendix2.

Assuming that the center temperature of solar panels is equal to air temperature.

In the night the energy change of PCM can be described in two ways:

$$dw = \frac{T_{PCM} - T_{air}}{R_{Top}} + 55.8\ dt \tag{27.1}$$

DOI: 10.54254/2755-2721/2025.28751

$$dw = C_p \times m\ dT \tag{27.2}$$

Connect these two equations together

$$\frac{T_{PCM}-T_{air}}{R_{Top}} + 55.8\ dt = C_p \times m\ dT \tag{28}$$

Integrate both sides of them.

$$\int_{18}^{T_{PCM\ orginal}} \frac{1}{T_{PCM}-T_{air}+55.8R_{panel-PCM}}\ dT = \int_0^t \frac{1}{C_p \times m \times R_{panel-PCM}}\ dt \tag{29}$$

$$\left[\ln\left(T_{PCM}-T_{air}+55.8R_{panel-PCM}\right)\right]_{18}^{T_{PCM\ orginal}} = \left[\frac{t}{C_p \times m \times R_{panel-PCM}}\right]_0^t \tag{30}$$

Since the formula is complex, R can be fixed by fixing the PCM temperature as the melting point temperature

The time for PCM to get melting point at night can be calculated and been put into Appendix2.

Assuming that the temperature varies with time linearly, it is reasonable to use the COP value at the midpoint of the temperature to represent the COP exceeds the median point temperature which is in Appendix2.

So, the average COP of these three locations can be calculated and showed in Table 3 below. (the operating time of air source COP was divided into day, which occupies $1/3$ and night which occupies $2/3$)

Table 3. COP of heat pump in three provinces

Parameter	Value
Heat pump COP with heat storage in Tibet	4.93
Heat pump COP with heat storage in Shaanxi	5.009
Heat pump COP with heat storage in Hainan	5.42
Heat pump COP with ambient air in Tibet	3.58
Heat pump COP with ambient air in Shaanxi	4.50
Heat pump COP with ambient air in Hainan	5.48

The n-Hexadecane (C_{16}) was gotten from HEBEI YANXI CHEMICAL CO., LTD which is 5 dollar per Kg [31].

So, the Unit capital expenditure of heat recovery facility can be calculated:

$$CAPEX_{HR} = \frac{cost\ of\ PCM}{Thermal\ storage\ capacity\ of\ PCM} = 0.0211\$/kW \tag{31}$$

The vacuum insulated panels come from Henan Jutao New Material Co., Ltd. [32], which is 53.33 dollar per m^2 . One solar panel needs vacuum insulated panels of 1.89 m^2

So, the Unit capital expenditure of heat storage facility can be calculated:

DOI: 10.54254/2755-2721/2025.28751

$$CAPEX_{HS} = \frac{cost\ of\ \text{vacuum insulated panels}}{Thermal\ storage\ capacity\ of\ PCM} = 0.00686\$/kJ \tag{32}$$

The cost of heat pump is 42847 dollars. So, the Unit capital expenditure of heat Pump can be calculated.

$$CAPEX_{HP} = \frac{cost\ of\ heat\ pump}{electric\ consumption} = 3839\$/kW \tag{33}$$

According to the equations, increasing the height of the PCM corresponding to each solar panel can significantly increase the convective heat transfer coefficient of the PCM. This not only reduces the number of solar panels required for each heat pump, but also increases heat recovery efficiency. However, this may increase the cost of PCM. If the new PCM thickness is calculated, it may result in a change in heat recovery efficiency, but the calculation method will try to maximize the heat recovery efficiency and thus minimize the number of solar panels needed for one heat pump. This may result in the COP of the heat pump not necessarily increasing when the number of PCMs is increased. Reducing the number of solar panels corresponding to a single heat pump without changing the PCM height can increase the COP.

3.3. Optimization model of the system

To determine parameters such as the power capacity of photovoltaic (PV) panels, the capacity of the battery energy storage system, and the capacity of the thermal energy storage system for the target region's photovoltaic combined heat and power (CHP) system, this study establishes a generalized optimization model. The team uses the annual photovoltaic capacity factor of the target region, annual electricity consumption data, and annual heating demand data as inputs to determine the system parameters. Through reasonable assumptions, simplification of physical processes, and relevant calculations, our research first define the objective function for the optimization problem.

Our research take cost minimization as the objective function of the optimization model, which consists of the costs of various subsystems. The costs of each subsystem are calculated by equations (34) as follows:

$$C_{PV} = CAPEX_{PV} \bullet Cap_{PV} \tag{34.1}$$

$$C_{HS} = CAPEX_{HS} \bullet Cap_{HS} \tag{34.2}$$

$$C_{BS} = CAPEX_{BS} \bullet Cap_{BS} \tag{34.3}$$

$$C_{HP} = CAPEX_{HP} \bullet Cap_{HP} \tag{34.4}$$

$$C_{HR} = CAPEX_{HR} \bullet Cap_{HR} \tag{34.5}$$

Here, C_{PV} , C_{HS} , C_{BS} , C_{HP} , and C_{HR} represent the total costs of the photovoltaic panels, thermal energy storage system, battery energy storage system, heat pump, and waste heat recovery unit, respectively. Their values are equal to the unit capital expenditure [33,34] multiplied by the total installed capacity. In this model, estimating the operational costs for remote areas is challenging, with significant errors and uncertainties. Therefore, to simplify the model and achieve a

DOI: 10.54254/2755-2721/2025.28751

more generalized optimization approach, our research primarily focus on the capital investment costs.

Accordingly, we express the objective function of this optimization model as follows:

$$C_{total} = C_{PV} + C_{HS} + C_{BS} + C_{HP} + C_{HR} \tag{35}$$

Next, we need to analyze the constraints of the optimization model. First, the energy balance of the electricity generated by the photovoltaic panels is subject to the following inequality and equality constraints (36):

$$P_{OPV} \leq PVData \bullet Cap_{PV} \tag{36.1}$$

$$P_{OPV} = P_{PVC} + P_{PVB} \tag{36.2}$$

Inequality (36.1) represents the constraint relationship between the total output power P_{OPV} of the photovoltaic system and the local photovoltaic input. Equation 222 represents the balance constraint between the total output power, energy consumption, and stored energy.

After determining the power balance of the solar photovoltaic panels, we need to analyze the supply and demand balance of the system. The power balance constraint (37) of the system are as follows:

$$P_{PVC} + P_{OB} \geq PowerDmandData + P_{HP} \tag{37}$$

P_{PVC} is the energy supplied to the load from the photovoltaic panels, and P_{OB} is the energy supplied to the load from the battery energy storage system. The sum of these two must cover the electricity demand on the user side as well as the electricity demand of the heat pump.

In order for the battery energy storage system to effectively perform peak shaving and valley filling, further constraints must be placed on the energy balance of the battery system. The energy balance (38) and capacity of the battery energy storage system (39) are expressed as follows:

$$Le_{BS}(t+1) = Le_{BS}(t) + \left(E_B \cdot P_{PVB}(t) - \frac{P_{OB}(t)}{E_B}\right) \cdot \Delta t \tag{38}$$

$$Cap_{BS} = Cap_{BSP} - Cap_{BSV} \tag{39}$$

Equation (38) reflects the change in the energy level of the battery energy storage system, where the energy level at the next time step $Le_{BS}(t)$ is equal to the energy level at the previous time step $L_{eBS}(t+1)$, plus the energy flowing in or out of the battery during that time period. It is important to note that for logical consistency and the safe operation of the battery pack, either $P_{PVB}(t)$ or $P_{OB}(t)$ must be positive at any given moment, while the other must be zero, meaning the battery system can either charge or discharge at any given time, but not both simultaneously. In the calculations, the time step Δt is set to one hour.

Next, we analyze the waste heat recovery process of the system. The relationship of the energy (power) recovered from the photovoltaic panels and stored in the thermal storage medium (40) is as follows:

DOI: 10.54254/2755-2721/2025.28751

$$P_{HIS} = \frac{P_{OPV}}{E_{PV}} (1 - E_{PV}) E_{hr} \tag{40}$$

The phase change material, after completing the waste heat recovery from the photovoltaic panels, will enter the storage tank. Therefore, the total power of the waste heat recovery is represented by P_{HIS}, which is the power input into the thermal storage system. Under the assumptions mentioned earlier, with a constant E_{PV}, the amount of solar energy converted into thermal energy can be derived from the energy balance equation. By multiplying this by the efficiency of the waste heat recovery system, the total waste heat recovery power is obtained.

Next, we analyze the heating situation provided by the heat pump. Assuming a constant COP_{HS}, the relationship between the energy supplied for heating from the thermal storage system and the power consumption of the heat pump is as follows:

$$P_{HOS} = P_{HPHS} \bullet (COP_{HS} - 1) \tag{41}$$

Here, P_{HOS} represents the energy output from the thermal storage system, and P_{HPHS} represents the power consumption of the heat pump. After determining the energy balance of the waste heat recovery and thermal storage systems, we need to analyze the supply and demand balance for the heating system. The heat balance constraint of the system (42) is as follows:

$$P_{HPHS} \bullet COP_{HS} + P_{PHAA} \bullet COP_{AA} \geq HeatDemandData \tag{42}$$

The above equation explains the relationship between the energy output from the thermal storage system, the energy generated by the air-source heat pump to compensate for the insufficient supply from the thermal storage system, and the heating demand.

To enable the thermal storage system to perform peak shaving and valley filling, further constraints must be applied to its energy balance. The energy balance and capacity of the thermal storage system (43) are expressed as follows:

$$P_{HPAA} \leq Cap_{HPAA} \tag{43.1}$$

$$P_{HPHS} \leq Cap_{HPHS} \tag{43.2}$$

$$P_{HIS} \leq Cap_{HR} \tag{43.3}$$

$$Le_{HS}(t+1) = Le_{HS}(t) + \left(E_{HS} \cdot P_{HIS}(t) - \frac{P_{HOS}(t)}{E_{HS}} \right) \cdot \Delta t \tag{44}$$

$$Cap_{HS} = Cap_{HSP} - Cap_{HSV} \# \tag{45}$$

Equations (43.1) and (43.2) represent the constraint relationship between the electrical power consumption of the heat pump and its rated power, while equation (43.3) represents the constraint relationship between the rated power of the waste heat recovery device and the waste heat recovery power.

Equation (44) illustrates the change in the energy level of the thermal storage system, where the storage level at the next time step $Le_{BS}(t)$ is equal to the storage level at the previous time step $Le_{BS}(t+1)$, plus the energy flowing in and out of the thermal storage tank during that time period.

DOI: 10.54254/2755-2721/2025.28751

Unlike battery energy storage systems, the thermal storage system does not require strict constraints on input and output power, meaning both can be positive at the same time. In the calculations, the time step Δt is set to one hour.

It should be noted that the designed optimization model assumes that both the battery energy storage system and the thermal storage system complete one full cycle of operation each day.

Based on our constraints and the objective function of the optimization model, it is clear that our optimization model is a linear programming problem. Therefore, our research attempt to use the interior point method to solve the optimization results. The interior point method is a type of mathematical algorithm used for solving constrained optimization problems, and it is particularly suitable for solving large-scale nonlinear optimization problems and linear programming problems. The solution process of the whole optimization model is presented in Fig. 4 as follows:

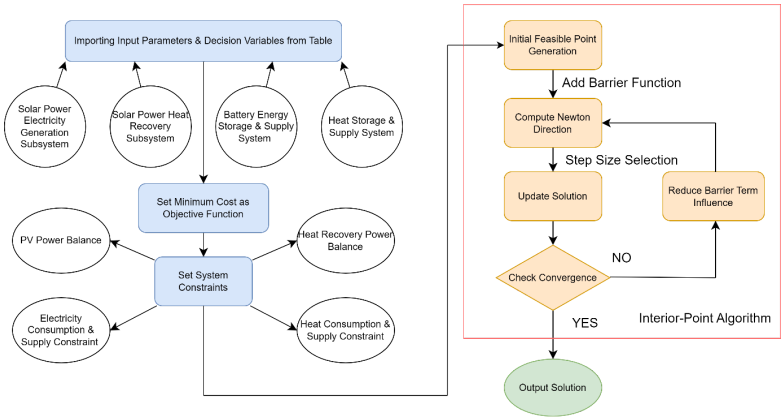

Figure 4. Solution process

4. Results & discussion

4.1. Optimization result of different provinces

In order to solve different input cases using our optimization model, our research programmed the system's mathematical model in MATLAB. Our research built an optimization model based on daily data, with precision down to each time period within 24 hours, incorporating power and solar radiation data. From the objective function and constraints of the optimization model, it is clear that both the objective function and all the constraints are linear. Therefore, our research used the linprog function in MATLAB. Another advantage of using the linprog function is that its default solving algorithm is the interior point method, which aligns with the algorithm preset in our optimization model, providing greater robustness to our model.

Our research input the electricity consumption data, heating demand data, and solar radiation data for Tibet, Shaanxi, and Hainan under the preset conditions into the program and solved the optimization results using the linprog function. The results provide the cost-minimizing photovoltaic combined heat and power (CHP) system construction plan for each province, meeting both electricity and heating demand. This includes the total installed capacity of photovoltaic panels, battery storage capacity, thermal storage system capacity, waste heat recovery system power capacity, heat pump power capacity, and total construction cost. The optimization models MATLAB as well as solar capacity factor, load, and heat data of three provinces are presented in Appendix3. The specific values are shown in the Table 4 below:

DOI: 10.54254/2755-2721/2025.28751

Table 4. Optimization results of three provinces

	Tibet	Shaanxi	Hainan
PV Capacity(kW)	1480	6480	3780
Battery Storage Capacity(kWh)	4880	7990	5760
Heat Storage Capacity(kWh)	1510	2120	642
Heat Recovery Capacity(kW)	375	945	708
Heat Pump Capacity(kW)	48.9	121	127.2
Total Cost(Million $)	4.3	8.6	6.5

It can be observed that the three provinces, with different climate conditions and energy demands, exhibit significant differences in the scale requirements for each subsystem. From the optimization results for photovoltaic (PV) panel installed capacity and battery storage capacity, our research can conclude the following:

1. Tibet has the smallest requirement for PV panel installed capacity. This is due to its lower average electricity demand compared to the other two provinces, as well as its consistently lower temperatures throughout the year, which results in higher PV panel efficiency than in other provinces.

2. Shaanxi has the highest demand for PV capacity, indicating a greater electricity requirement in the region. This is linked to its relatively high level of industrialization and corresponding electricity demand.

3. There is a positive correlation between the relative size of the Battery Storage Capacity in the three provinces and the installed capacity of the PV panels.

In terms of Heat Storage Capacity, it is evident that Hainan has the smallest installed capacity. This is mainly because it is located in a low-latitude region with consistently mild temperatures, which results in relatively low heating demand. Although Tibet has a significantly smaller PV panel installed capacity compared to Shaanxi, its Heat Storage Capacity is not considerably lower than that of Shaanxi. This is primarily due to Tibet's much higher heating demand compared to the other two provinces.

Moreover, considering the coefficients of performance (COP) of both the waste heat recovery system’s heat pump and the air-source heat pump, which are largely influenced by climatic factors, in low-latitude subtropical provinces like Hainan, the higher temperatures mean that the COP of the heat pump using waste heat recovery from PV panels is not much greater than the COP of the air-source heat pump, and thus, the advantage is not significant. This leads to a noticeably higher heat pump demand in Hainan than in the other provinces.

Additionally, based on the results from the daily optimization model, our research calculated the average daily battery storage levels and heat storage levels for each month, resulting in monthly average daily peak battery storage (consumption) level and heat storage (consumption) levels over the year for the three provinces. The bar charts depicting these variations are shown in Fig. 5 and Fig. 6 below:

DOI: 10.54254/2755-2721/2025.28751

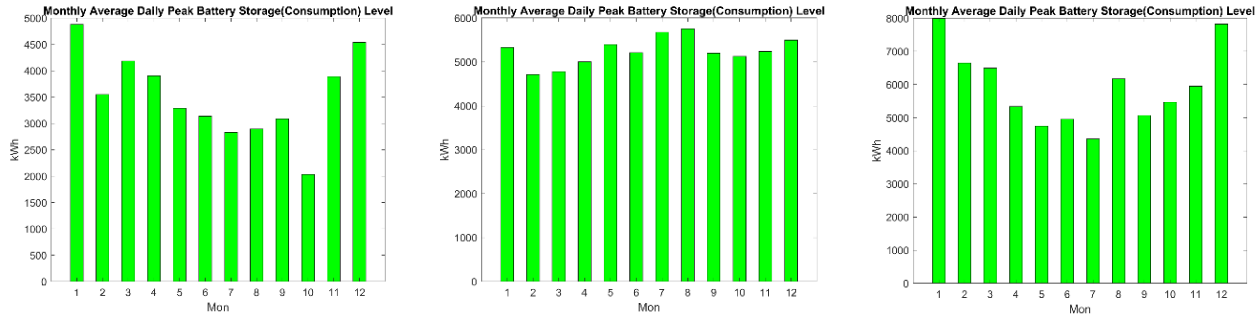

(a) Tibet's (b) Hainan's (c) Shaanxi's

Figure 5. Monthly average daily peak battery storage (consumption) level of three provinces

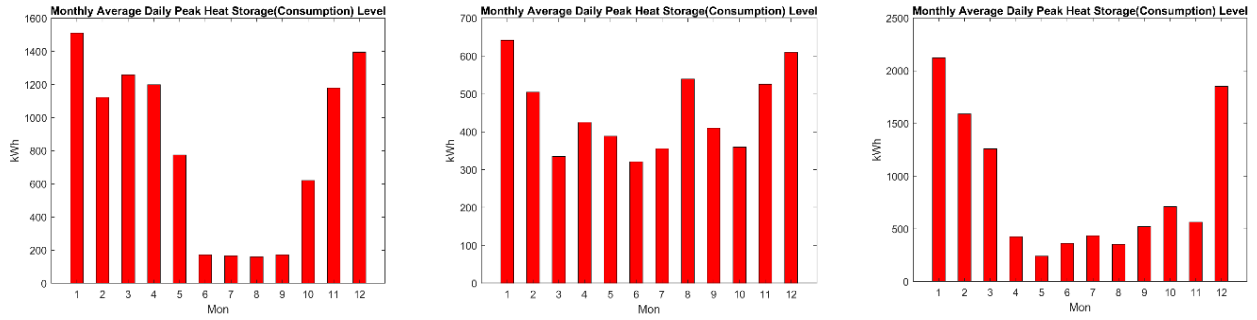

(a) Tibet's (b) Hainan's (c) Shaanxi's

Figure 6. Monthly average daily peak heat storage (consumption) level of three provinces

We can observe that the changes in peak battery storage (consumption) levels in the three provinces correspond to their respective electricity demand curves. Under the premise of a once-daily cycle, the monthly average daily peak battery storage (consumption) reflects the amount of photovoltaic energy generated but not used in time, which is stored and later used when the photovoltaic system's power cannot meet the load demand within the day. By considering the average daily levels over the twelve months, our research use this as a basis for designing the capacity scale of the battery storage system.

Regarding the changes in peak heat storage (consumption) levels, our optimization results show that the model can effectively track the heating demand of different provinces to design appropriate thermal storage capacities and waste heat recovery systems. Our research observe that the heat storage levels remain relatively low between May and September, as temperatures rise during this period, reducing heating demand. Conversely, from November to February, as temperatures drop, the peak heat storage (consumption) levels reach their highest points of the year.

4.2. Efficiency improvement and optimization results of different systems

Based on the previous calculations, our research designed the waste heat recovery system using a 50mm PCM (phase change material) thickness, obtaining the performance parameters of the system with the added PCM waste heat recovery device, including the efficiency of the photovoltaic panels and the COP of the thermal storage heat pump, among others. To verify the efficiency and cost-effectiveness of our designed system, our research selected typical electricity and heating demand

DOI: 10.54254/2755-2721/2025.28751

data for a day in February in the Tibet province, along with the corresponding solar radiation data for that day, as input for the daily optimization model of our designed system. At the same time, we input the same data into the daily optimization model for a system without the waste heat recovery device, to compare the differences between the two systems in terms of cost, efficiency, and other factors. It is important to note that in the system without the waste heat recovery device, the heating demand will be fully met using electricity, meaning that the electricity demand data in this case is the sum of the original electricity demand data and the heating demand data.

The optimization results for both systems under the respective models are as follows in Table 5:

Table 5. Comparison between systems with and without heat recovery

	With Heat recovery(50mm)	Without Heat Recovery
PV Capacity(kW)	750.1092	1130
PV Efficiency	0.157	0.155
Battery Storage Capacity(kWh)	3551	5159
Heat storage capacity(kWh)	1120	-
Heat Pump Capacity(kW)	40.1	-
Heat Recovery Capacity(kW)	224.7432	-
Total Cost(Million Dollars)	2.26	3.23

As we can see, compared to the standard photovoltaic system without the waste heat recovery device, our designed system, while not significantly improving photovoltaic efficiency, achieves a substantial reduction in overall electricity consumption by using the waste heat recovery system to meet heating demand. This is made possible by the high COP (Coefficient of Performance) of the heat pump. In contrast to the relatively expensive photovoltaic panels and battery storage systems, the low cost and scalability of phase change thermal storage materials provide a clear advantage when designing such microgrid systems. According to the optimization results, our designed photovoltaic combined heat and power (CHP) system can reduce costs by approximately 30% compared to traditional photovoltaic systems.

Additionally, our research obtained the changes in battery storage levels throughout the day for both model with heat recovery and without heat recovery, as shown in the Fig. 7.

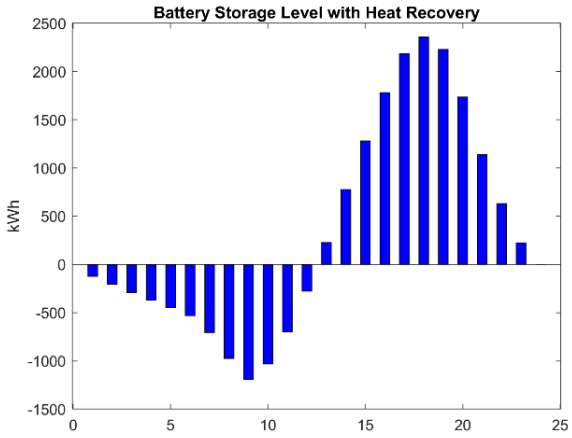

(a) With heat recovery

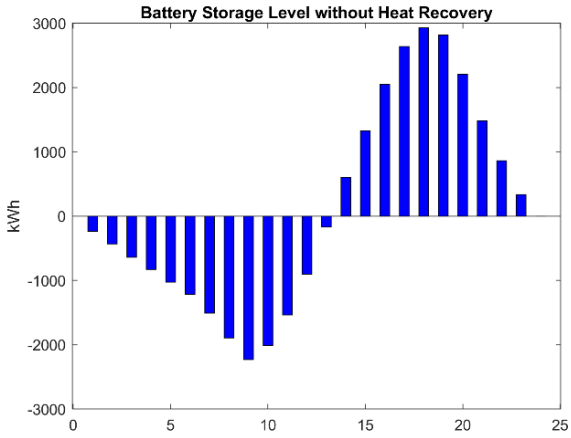

(b) Without heat recovery

DOI: 10.54254/2755-2721/2025.28751

Figure 7. Comparison of hourly battery storage level of a day in Feb. in Tibet

In the graph, the periods where the battery storage level is negative indicate that the power supply during those times requires support from external sources beyond the microgrid photovoltaic system.

At the same time, following the calculation approach in section 3.1, our research designed a system with a 100mm PCM thickness, and the corresponding data is as follows in Table 6:

Table 6. 100mm PCM system parameters

Parameter	Value
The mass of PCM for one solar panel (kg)	124
Temperature difference from panels to PCM (℃)	9.94
Cell temperature in Tibet (℃)	289.98
Cell temperature in Shaanxi (℃)	35.13
Cell temperature in Hainan (℃)	39.74
Efficiency of PV panels in Tibet (%)	15.71
Efficiency of PV panels in Shaanxi (%)	15.53
Efficiency of PV panels in Hainan (%)	14.94
Efficiency of heat recovery in Tibet (%)	8.79
Efficiency of heat recovery in Shaanxi (%)	13.16
Efficiency of heat recovery in Hainan (%)	14.41
Heat pump COP with heat storage in Tibet	4.91
Heat pump COP with heat storage in Shaanxi	4.99
Heat pump COP with heat storage in Hainan	5.31

5. Conclusion and outlook

This study proposes a photovoltaic-thermal cogeneration system and constructs its optimization model, offering a solution to the energy supply challenges in remote areas. The system significantly enhances energy efficiency by integrating photovoltaic (PV) panels with phase-change materials (PCM) for heat recovery, battery energy storage, and heat pumps. Tested in regions with varying climatic conditions and energy demands, such as Tibet, Shaanxi, and Hainan, the system has demonstrated good scalability and cost-effectiveness.

Key results indicate that, compared to traditional PV systems, this system can reduce total costs by approximately 30% while meeting the heating and electricity demands of remote areas. Specifically, in Tibet, with the designed sample capacity, the required PV installation capacity is lower (1480 kW) due to higher PV panel efficiency in colder climates, while Shaanxi, with higher energy demand, requires a capacity of 6480 kW.

By mitigating heat accumulation, the system improves the electrical efficiency of PV panels. For instance, the study showed that using PCM to maintain lower operating temperatures improved PV panel efficiency in provinces like Tibet, Shaanxi, and Hainan. In Tibet, the efficiency of PV panels with a 50mm PCM design was 15.65%, and with a 100mm PCM design, it increased to 15.71%, slightly higher than traditional systems without heat recovery, which have lower efficiency due to heat buildup. The introduction of PCM heat recovery not only enhances PV panel efficiency but also

DOI: 10.54254/2755-2721/2025.28751

meets heating demands, particularly in colder regions, further improving energy utilization. Additionally, the system improves the coefficient of performance (COP) of heat pumps. For example, the COP in Tibet reaches 4.93, while in Hainan, it reaches 5.42.

Overall, the PV-T cogeneration system successfully demonstrates scalability, economic feasibility, and optimized energy efficiency in remote areas by combining solar power generation with heat recovery and storage technologies. These findings contribute to advancing renewable energy solutions for areas with insufficient grid coverage.

However, there are several limitations and areas for improvement in this research. For example, the reliability and maintenance of the system during long-term operation have not been fully addressed. While the system performed well in short-term experiments, maintenance needs, component aging, and the actual lifespan of the system in long-term operation have not been thoroughly discussed. Future studies could conduct long-term monitoring and evaluation of the system to explore maintenance costs and system reliability. Another issue is the limitations of heat pump performance. Although the COP of heat pumps shows good efficiency in different regions, the system's performance under extreme climate conditions, such as very high or very low temperatures, has not been fully explored. Future research could optimize the design of heat pumps, particularly for high-altitude or extreme climate regions, to further enhance system efficiency and reliability.

Acknowledgments

The study was conducted under the supervision of Professor Aidong Yang of the University of Oxford. Professor Yang gave the team a lot of key guidance and inspiration during the research. Also, we would like to thank Zhishang Wu from Monash University, who has provided many research resources to our team.

Yonghan Jiao, Yunting Du, and Zhifan Ye contributed equally to this work and should be considered co-first authors.

References

[1] Tan, Y., Meegahapola, L., & Muttaqi, K. M. (2014). A review of technical challenges in planning and operation of remote area power supply systems. Renewable and Sustainable Energy Reviews, 38, 876–889. https: //doi.org/10.1016/j.rser.2014.07.034

[2] Ryan, N. (2021). The competitive effects of transmission infrastructure in the Indian electricity market. American Economic Journal Microeconomics, 13(2), 202–242. https: //doi.org/10.1257/mic.20180191

[3] Ettappan, M., Vimala, V., Ramesh, S., & Kesavan, V. T. (2020). Optimal reactive power dispatch for real power loss minimization and voltage stability enhancement using Artificial Bee Colony Algorithm. Microprocessors and Microsystems, 76, 103085. https: //doi.org/10.1016/j.micpro.2020.103085

[4] Lin, B., & Wu, W. (2017). Cost of long distance electricity transmission in China. Energy Policy, 109, 132–140. https: //doi.org/10.1016/j.enpol.2017.06.055

[5] Tian, J., Zhou, S., & Wang, Y. (2023). Assessing the technical and economic potential of wind and solar energy in China—A provincial-scale analysis. Environmental Impact Assessment Review, 102, 107161. https: //doi.org/10.1016/j.eiar.2023.107161

[6] Li, J., Chen, S., Wu, Y., Wang, Q., Liu, X., Qi, L., Lu, X., & Gao, L. (2020). How to make better use of intermittent and variable energy? A review of wind and photovoltaic power consumption in China. Renewable and Sustainable Energy Reviews, 137, 110626. https: //doi.org/10.1016/j.rser.2020.110626

[7] Sharaf, M., Yousef, M. S., & Huzayyin, A. S. (2022). Review of cooling techniques used to enhance the efficiency of photovoltaic power systems. Environmental Science and Pollution Research, 29(18), 26131–26159. https: //doi.org/10.1007/s11356-022-18719-9

[8] Elavarasan, R. M., Mudgal, V., Selvamanohar, L., Wang, K., Huang, G., Shafiullah, G., Markides, C. N., Reddy, K., & Nadarajah, M. (2022). Pathways toward high-efficiency solar photovoltaic thermal management for electrical,

DOI: 10.54254/2755-2721/2025.28751

thermal and combined generation applications: A critical review. Energy Conversion and Management, 255, 115278. https: //doi.org/10.1016/j.enconman.2022.115278
[9] Sheikholeslami, M., & Khalili, Z. (2024). Enhancing photovoltaic solar panel performance with integration of PCM-based spectral filter and self-cleaning coating. Journal of Building Engineering, 94, 110019. https: //doi.org/10.1016/j.jobe.2024.110019
[10] Xuewei, S., Xuefang, S., Wenqi, D., Peng, Z., Hongyan, J., Jinfang, W., & Yang, W. (2020). Research on Energy Storage Configuration Method based on wind and solar volatility. 2020 10th International Conference on Power and Energy Systems (ICPES). https: //doi.org/10.1109/icpes51309.2020.9349645
[11] Liang, J., Irfan, M., Ikram, M., & Zimon, D. (2022). Evaluating natural resources volatility in an emerging economy: The influence of solar energy development barriers. Resources Policy, 78, 102858. https: //doi.org/10.1016/j.resourpol.2022.102858
[12] Vakhshouri, A. R. (2019). Paraffin as phase change material. In IntechOpen eBooks. https: //doi.org/10.5772/intechopen.90487
[13] Li, J., Chen, S., Wu, Y., Wang, Q., Liu, X., Qi, L., ... & Gao, L. (2021). How to make better use of intermittent and variable energy? A review of wind and photovoltaic power consumption in China. Renewable and Sustainable Energy Reviews, 137, 110626. https: //doi.org/10.1016/j.rser.2020.110626
[14] Shi, J., Cui, L, Tian, Z., & Yu, Q. (2011). Impact of temperature change on heating and cooling energy consumption of residential buildings in East China. Journal of Natural Resources, 26(3), 460-467. https: //doi.org/10.11849/zrzyxb.2011.03.012
[15] Zhang, L., Li, Y., Zhang, H., Xu, X., Yang, Z., & Xu, W. (2021). A review of the potential of district heating system in Northern China. Applied Thermal Engineering, 188, 116605. https: //doi.org/10.1016/j.applthermaleng.2021.116605
[16] Su, F., Chang, J., Li, X., Fahad, S., & Ozturk, I. (2023). Assessment of diverse energy consumption structure and social capital: A case of southern Shaanxi province China. Energy, 262, 125506. https: //doi.org/10.1016/j.energy.2022.125506
[17] Zhang, P., Wang, Y., Yu, Z., Shao, X., & Chong, H.-Y. (2024). Analysis of the Spatio-Temporal Differences and Structural Evolution of Xizang's County Economy. Sustainability, 16(18), 7937. https: //doi.org/10.3390/su16187937
[18] NDRC. (2020). Typical power curve of each provincial power grid. https: //www.ndrc.gov.cn/xwdt/tzgg/202012/P020201202546044875868.pdf
[19] Renewables.ninja. (n.d.). https: //www.renewables.ninja/
[20] Solimpeks Enerji Paz. Ltd. Şti., Solimpeks Solar SL., & Solimpeks Solarenergie GmbH. (n.d.-b). Solimpeks. https: //solimpeks.com.tr/wpcontent/uploads/Solimpeks_English_Catalogue.pdf
[21] Nominal Operating cell Temperature | PVEDucation. (n.d.). https: //www.pveducation.org/pvcdrom/modules-and-arrays/nominal-operating-cell-temperature
[22] Marsh, J. (2020). How hot do solar panels get? PV temperature explained. EnergySage. https: //www.energysage.com/solar/solar-panel-temperature-overheating/
[23] Editor Engineeringtoolbox. (2024). Convective heat transfer. https: //www.engineeringtoolbox.com/convective-heat-transfer-d_430.html
[24] Aggarwal, V., & Walker, E. (2024). How do solar panels work? Solar Power explained. EnergySage. https: //www.energysage.com/solar/solar-panels-work/#how-solar-panels-work-the-photovoltaic-effect-explained
[25] A Heat Transfer Textbook, 6th edition. (n.d.). https: //ahtt.mit.edu/
[26] Cherif, Y., Zalewski, L., Sassine, E., & Groulx, D. (2024). Use of the inverse method to determine the thermal properties of liquid n-octadecane accounting for natural convection effect. International Journal of Heat and Mass Transfer, 231, 125864. https: //doi.org/10.1016/j.ijheatmasstransfer.2024.125864
[27] Kumar, B., Awasthi, A., Suresh, C., & Jeon, Y. (2023). Novel effective thermal conductivity numerical model for distinct shaped pure paraffins (C14–C33). Journal of Energy Storage, 76, 109654. https: //doi.org/10.1016/j.est.2023.109654
[28] Cetene (CAS 629-73-2). (n.d.). Cheméo. https: //www.chemeo.com/cid/45-407-0/Cetene
[29] Vitocal 300-A air source heat pump (47 kW) | Viessmann AE. (2024). https: //www.viessmann.ae/en/products/heat-pump/vitocal-300-a.html
[30] Oehm, C., & Oehm, C. (2023). Do solar panels reflect light? ShopSolar.com. https: //shopsolarkits.com/blogs/learning-center/do-solar-panels-reflect-light
[31] Hexadecane | China | Manufacturer | Hebei Yanxi Chemical Co., Ltd. (n.d.). Chemicalbook. https: //www.chemicalbook.com/ProductDetail_EN_n-hexadecane-d34_2429721.htm

DOI: 10.54254/2755-2721/2025.28751

[32] Henan Jutao New Material Co., Ltd. (n.d.). 2023 Most popular VIP vacuum insulation panel. www.alibaba.com. https: //www.alibaba.com/product-detail/2023-Most-Popular-VIP-Vacuum-Insulation_1600745400260.html?spm=a2700.shop_cp.61684.8.4a71d49c5qzvkg
[33] Cole, W., & Karmakar, A. (2023). Cost projections for Utility-Scale battery Storage: 2023 update. https: //doi.org/10.2172/1984976
[34] IRENA (2023), Renewable power generation costs in 2022, International Renewable Energy Agency, Abu Dhabi.